Bioorganic & Medicinal Chemistry Letters 22 (2012) 3011–3016

Contents lists available at SciVerse ScienceDirect

Bioorganic & Medicinal Chemistry Letters

journal homepage: www.elsevier.com/locate/bmcl

Footprint-based identification of viral entry inhibitors targeting HIVgp41

Patrick M. Holden [a], Harmeet Kaur [b], Rashi Goyal [c], Miriam Gochin [b,d], Robert C. Rizzo [a,e,*]

[a] Department of Applied Mathematics and Statistics, Stony Brook University, Stony Brook, NY 11794, USA
[b] Department of Basic Sciences, Touro University—California, 1310 Johnson Lane, Mare Island, Vallejo, CA 94592, USA
[c] Department of Biomedical Engineering, Stony Brook University, Stony Brook, NY 11794, USA
[d] Department of Pharmaceutical Chemistry, University of California San Francisco, CA 94143, USA
[e] Institute of Chemical Biology and Drug Discovery, Stony Brook University, Stony Brook, NY 11794, USA

ARTICLE INFO

Article history:
Received 4 January 2012
Accepted 6 February 2012
Available online 16 February 2012

Keywords:
HIVgp41
Virtual screening
Structure-based drug design
Molecular footprints
Pose rescoring
Docking
DOCK

ABSTRACT

A targeted virtual screen to the N-helix hydrophobic pocket on HIVgp41 was performed using DOCK followed by re-ranking with a new footprint-based scoring function which employed native gp41 C-helix residues as a reference. Of ca. 500,000 small molecules screened, 115 were purchased, and 7 hits were identified with favorable binding (K_i), cell–cell fusion (IC_{50}), and cytotoxicity (CC_{50}) profiles. Three of the seven active compounds would not have been discovered without the use of the footprints, demonstrating the utility of the method for structure-based design when a known reference compound or substrate is available.

The HIV glycoprotein (HIVgp41) is a validated viral entry drug target with one FDA approved inhibitor, a 36 a.a. peptide known as T20 (FUZEON).[1] Despite the success of T20 as a first-in-class fusion inhibitor, there are known resistance problems, it is expensive to produce (ca. USD $25,000 per person per year), and it must be delivered via injection.[1–5] An effective small molecule gp41 inhibitor would be an important addition to the arsenal of compounds used to treat HIV/AIDS. A highly conserved hydrophobic pocket, adjacent to the putative T20 binding interface,[6] was previously identified as a likely drug target.[7] Active small molecules, presumably targeting the pocket, have been reported (see Cai and Jiang[8] for a recent review), although specific binding poses have not yet been confirmed by crystallography. Compounds have been discovered using traditional high-throughput, NMR, and computer-based screening.[8,9] Most small molecule leads have been in the μM range although some have been reported with activities that are sub-μM.[10,11] The extent of the HIV/AIDS pandemic necessitates continued screening and development of new inhibitors targeting gp41.

In this work, we have taken a computational screening approach which employs a novel molecular footprint comparison rescoring method[12] recently implemented by our laboratory into the program DOCK6.5.[13] Footprint comparisons employ per-residue decompositions of the standard DOCK energy score to compare docked molecules with a known reference as illustrated in Figure 1. Balius et al.[12] have shown that footprint-guided selection enhances success for reproducing known binding geometries (poses). We hypothesize that screening for compounds which make footprints similar to a reference known to bind gp41 will facilitate discovery of anti-gp41 inhibitors.

The gp41 reference used for rescoring in this study is based on the native gp41 C-helix reduced to four key sidechains, Trp117, Trp120, Asp121 and Ile124 (gp41 numbering), that interact with the conserved hydrophobic pocket. Figure 1 shows the van der Waals (VDW) footprint derived from the crystallographic reference 1AIK[14] (green), in comparison to the VDW footprint from a representative docked ligand (magenta), taken from the virtual screen. The periodicity in the footprints reflects the α-helical nature of the target and the strongest peaks indicate residues which interact most favorably with either the reference, the docked molecule, or both. Importantly, this example demonstrates how footprint overlap can be used as a means to identify compounds that make similar interactions with gp41 as a known reference, in terms of both a.a. position and energetic strength.

Throughout this study footprint overlap is quantified using a Pearson correlation coefficient and termed footprint similarity (FPS) score, although other metrics such as Euclidian distance may be used.[12] In addition to the VDW example in Figure 1 (FPS_{VDW} = 0.97), electrostatic interactions (FPS_{ES}) computed from Coulombic energies scaled by a distance dependent dielectric, as well as the combined sum (FPS_{VDW+ES}), were also employed. In particular, significant electrostatic interactions in this system are

* Corresponding author.
E-mail address: rizzorc@gmail.com (R.C. Rizzo).

0960-894X/$ - see front matter © 2012 Elsevier Ltd. All rights reserved.
doi:10.1016/j.bmcl.2012.02.017

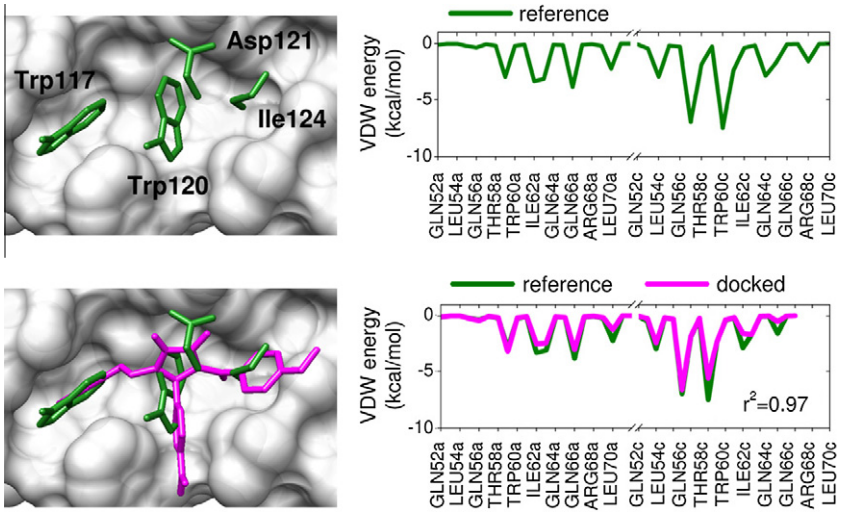

Figure 1. (top) Key C-helix residues of the gp41 reference and associated VDW footprint in green. (bottom) Comparison between a docked ligand (magenta) and the reference (green).

observed between Asp121 (C-helix) and Lys63a (N-helix chain (a)) which are known to be important for binding.[15] By using footprint comparisons to help guide the search, molecules making similar interactions can be selected over others.

A comprehensive virtual screen of ca. 500,000 compounds was performed using DOCK6.5. The docking database was taken from the ZINC library (http://zinc.docking.org) of commercially-available compounds for virtual screening.[16] As shown in Figure 2, each compound was flexibly docked to the gp41 receptor grid (DOCK FLX protocol)[17] and the single lowest-energy pose was retained. The docking grid was generated from the gp41 crystal structure 1AIK[14] using only the trimeric N-helix core. After docking, the FPS scores were calculated between each energy minimized compound and the C-helix derived reference (Fig. 2). The top 100,000 molecules (energy score) were then clustered, using MACCS fingerprints,[18] as implemented in the program MOE[19] using a tanimoto coefficient of 0.75. The best scoring member of each cluster (i.e., clusterhead) was retained for subsequent steps to increase the overall chemical diversity of the compounds ultimately selected for purchase.

The resultant clusterheads (ca. 56,500) were then rank-ordered using four different scoring methods: (i) standard DOCK score (DCE_{VDW+ES}), (ii) van der Waals footprint similarity score (FPS_{VDW}), (iii) electrostatic footprint similarity score (FPS_{ES}), and (iv) the combined footprint sum (FPS_{VDW+ES}). The top 500 compounds obtained by each method were retained (Fig. 3) and after visual inspection a subset from each of the ranked lists was selected for purchase and experimental testing. An effort was made during the selection process to choose a diverse set of molecules with favorable properties among several categories.

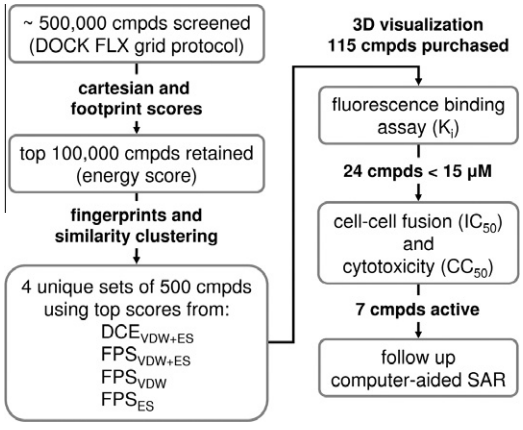

Figure 2. Virtual screening and experimental evaluation workflow.

Importantly, each group of 500 top ranked molecules obtained by different scoring methods (DCE_{VDW+ES} = black, FPS_{VDW+ES} = orange, FPS_{VDW} = green, FPS_{ES} = blue) has a different set of characteristics as shown by the histograms in Figure 3 which plot (a) DCE_{VDW+ES} scores, (b) molecular weight, (c) number of rotatable bonds, (d) FPS_{VDW+ES} scores, (e) FPS_{VDW} scores, and (f) FPS_{ES} scores. As expected, molecules selected using a particular scoring function will have the most favorable scores, relative to other sets, when viewed in the accompanying histogram. For example, molecules picked using DCE_{VDW+ES} generally have more favorable DCE_{VDW+ES} scores (Fig. 3a, black line). Likewise, molecules picked using FPS_{VDW+ES} have more favorable FPS_{VDW+ES} scores (Fig. 3d, orange line). Not surprisingly, molecules chosen using FPS_{VDW+ES} (orange line) also show enhanced populations in the FPS_{VDW} and FPS_{ES} histograms. As a baseline, the computed DCE_{VDW+ES} energy score for the reference (Fig. 1) is −46.36 kcal/mol which interestingly is at the intersection (Fig. 3a) of the DCE (upper) and FPS (lower) score ranges.

Compounds chosen using DCE_{VDW+ES} generally have more favorable DCE_{VDW+ES} scores than those chosen using FPS methods which is understandable when one considers that molecules chosen using DCE_{VDW+ES} also have higher MW (Fig. 3b black vs other colors), a known scoring bias problem in DOCK. In contrast, use of FPS yields a wider range of MW, which on average, are also lower: DCE_{VDW+ES} = 483.2 g/mol versus FPS_{VDW} = 456.8 g/mol, FPS_{ES} = 415.1 g/mol, FPS_{VDW+ES} = 432.2 g/mol. In general, use of FPS also results in molecules with lower numbers of rotatable bonds which indicate more rigid, potentially more drug-like, lead molecules (Fig. 3c black versus other colors).

Following selection protocols, a total of 115 compounds were purchased. Compounds were tested in a fluorescence-based binding assay (K_i),[20] and those that displayed activity were evaluated in follow-up cell–cell fusion (IC_{50}), and cytotoxicity assays (CC_{50}) as previously described in Zhou et al.[11] Encouragingly, 24 molecules showed binding with K_i values <15 μM. Importantly, 18 out of the 24 were selected using FPS scoring. Ultimately, 7 compounds were identified as having favorable properties (low K_i, low IC_{50}, high CC_{50}) in all three assays and are termed here 'actives'

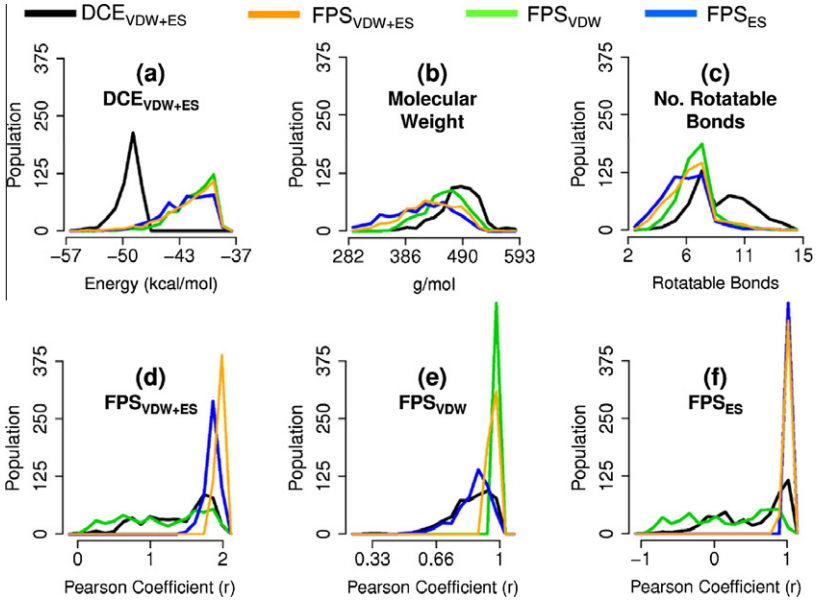

Figure 3. Histograms of **(a)** DCE_{VDW+ES} score, **(b)** molecular weight, **(c)** number of rotatable bonds, **(d)** FPS_{VDW+ES} score, **(e)** FPS_{VDW} score, and **(f)** FPS_{ES} score from the different ensembles of 500 molecules obtained from each of the four ranking methodologies: DCE_{VDW+ES} = black, FPS_{VDW+ES} = orange, FPS_{VDW} = green, FPS_{ES} = blue.

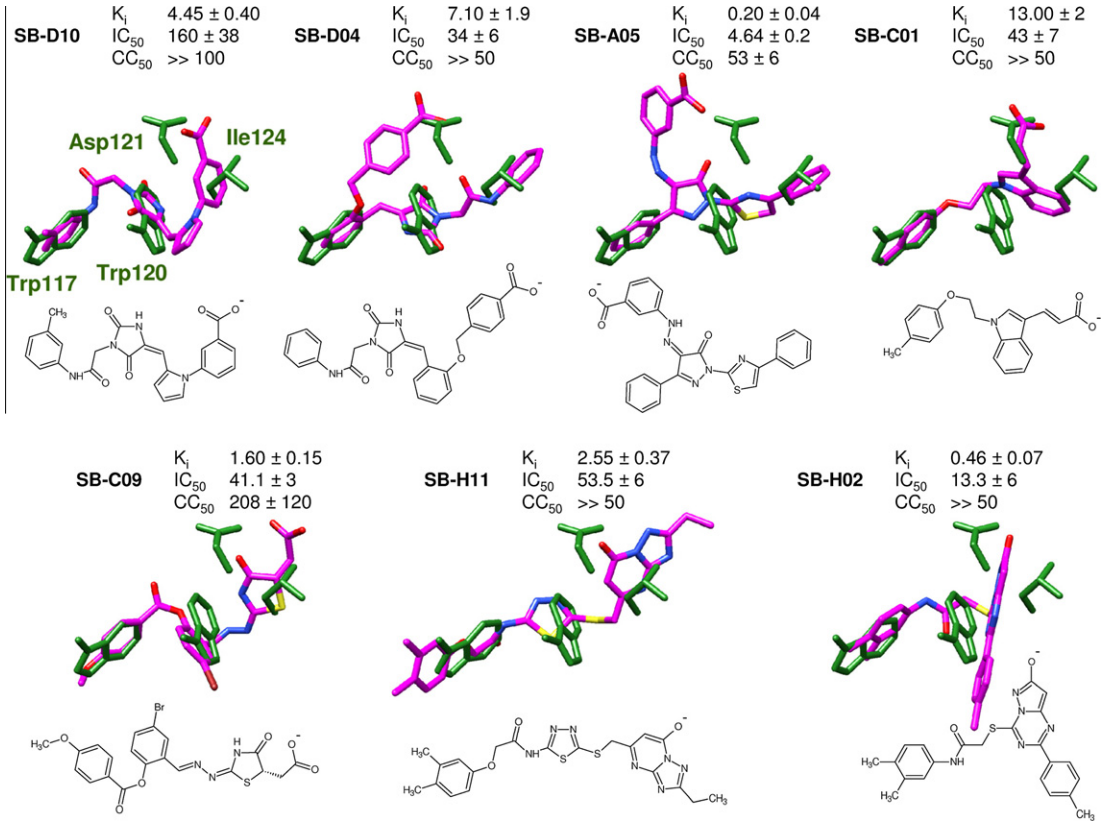

Figure 4. Predicted binding modes for 7 active compounds (magenta) in comparison with the reference sidechains (green). Activities in μM determined using fluorescence binding (K_i), cell–cell fusion (IC_{50}), and cytotoxicity (CC_{50}) assays as previously described in Zhou et al.[11]

(Fig. 4, Table 1). It should be emphasized that 3 of the 7 actives (**SB-D10**, **C01**, and **H02**) would not have been chosen for experimental testing without the use of footprints because their DCE_{VDW+ES} scores, while close to that of the reference, were not favorable enough to be within the top 500 molecules. For example, **SB-C01** ranked 27,427th by DCE_{VDW+ES} score and thus in a traditional virtual screen would have been discarded. Through its similarity in electrostatic interactions to the reference the rank dropped to 247th in the list of FPS_{ES} clusterheads and was ultimately selected for purchase.

It should be emphasized that during compound selection, priority was also given if a ligand showed favorable scores in more

Table 1
Primary selection method and virtual screening scores

ID[a]	Method[b]	DCE_{VDW+ES}	FPS_{VDW+ES}	FPS_{VDW}	FPS_{ES}
SB-D10	FPS_{ES}	−43.85	1.90	0.91	0.99
SB-D04	DCE_{VDW+ES}	−50.86	1.90	0.91	0.98
SB-C01	FPS_{ES}	−41.86	1.90	0.90	0.99
SB-A05	DCE_{VDW+ES}	−51.51	1.82	0.84	0.98
SB-C09	DCE_{VDW+ES}	−51.48	1.97	0.98	0.99
SB-H11	DCE_{VDW+ES}	−52.10	1.84	0.86	0.99
SB-H02	FPS_{VDW+ES}	−44.33	1.96	0.97	0.99
RG-1 (29)	DCE_{VDW+ES}	−51.93	1.67	0.89	0.78
RG-2 (21)	FPS_{VDW+ES}	−43.54	1.96	0.98	0.99
RG-3 (33)	FPS_{VDW}	−42.25	1.08	0.99	0.09
RG-4 (32)	FPS_{ES}	−43.81	1.88	0.88	0.99
SB-avg		−48.00	1.90	0.91	0.99
RG-avg		−45.38	1.65	0.94	0.71
CH-ref		−46.36	2.00	1.00	1.00

[a] SB prefix designates active molecules, RG prefix designates ensembles based on the four different ranking methods. CH-ref designates reference molecule based on C-helix sidechains.
[b] DCE scores in kcal/mol, FPS scores are unitless.

than one category. As a result, each of the four Ranked Groups (RG prefix, Table 1), for the most part, also showed reasonable high average scores across all scoring methods. Only the FPS_{VDW} group (RG-3) yielded poor FPS_{ES} scores (0.09) and consequently lower FPS_{VDW+ES} scores (1.08). Notably, on average, the 7 actives (SB-avg, Table 1) have more favorable scores than the total group of 115 tested (RG-avg in Table 1) in three out of four categories (DCE_{VDW+ES}, FPS_{VDW+ES}, and FPS_{ES}) and more closely approach the reference values (CH-ref, Table 1).

Of the actives, **SB-C09** was ranked in the top 500 by DCE_{VDW+ES}, FPS_{ES}, and FPS_{VDW+ES} methods. If the group size is expanded to the top 2000, then **SB-C09**, **SB-D04**, **SB-A05**, and **SB-H11** are all ranked in at least one additional category. Given that these four compounds are all active provides evidence that an intersection of good scores from the different rankings methods (i.e., consensus scoring) is a reasonable protocol for prioritizing compounds. Within the top 2000 ranked using DCE_{VDW+ES}, 68 ligands are in the top FPS_{VDW}, 181 are in the top FPS_{ES}, and 104 are in the top FPS_{VDW+ES}.

As highlighted in Figure 4, the 7 actives have a number of intra and intermolecular structural features in common. All have a formal charge of −1 and five have a carboxylic acid which is predicted to interact with Lys63a of gp41 in a manner analogous to Asp121 of the reference. This salt-bridge is considered to be an important feature of many inhibitors.[15] The actives are also dominated by the presence of planar aromatic rings which occupy positions in the pocket normally occupied by the reference sidechains (Fig. 4 green vs magenta). In particular, all compounds have significant ring overlap with Trp117. Prior work by our laboratory[21] quantified the importance of Trp117 and Trp120 which together make up the bulk of the VDW interactions in the pocket.

Structurally, several actives have features in common with other reported gp41 inhibitors. For example, compound **SB-D10** contains an N-substituted pyrrole group (see Fig. 4) similar to the NB-2 and NB-64 inhibitors reported by Jiang et al.[22] And, the general size and layout of **SB-D10** is roughly similar to a group of analogs reported by Katritzky et al[10] which were designed around the pyrrole functionality to more completely fill the hydrophobic pocket. **SB-D10** also shares significant chemical similarity with **SB-D04** although interestingly the 3D poses are ca. 180° flipped (Fig. 4). To probe if either compound could adopt the pose adopted by the other, a series of additional docking runs were performed. Figure 5 shows two possible low-energy poses with higher structural overlap than that illustrated in Figure 4. Interestingly, although the best alternative pose shown for **SB-D04** (Fig. 5, pose #1, orange) has a less favorable DCE_{VDW+ES} score (−41.36 vs −50.86 kcal/mol) the larger FPS_{VDW} (0.94 vs 0.91) and FPS_{ES} (0.99 vs 0.98) scores indicate improved overlap with the C-helix reference footprints (Table 1). Additional studies, including MD refinement (see discussion below), are in progress.

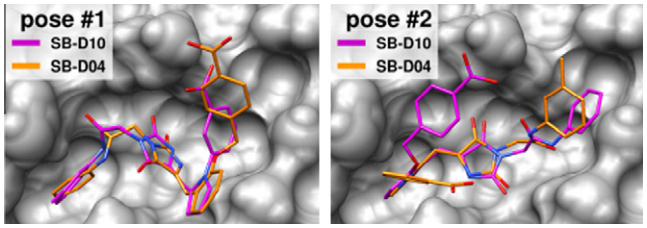

Figure 5. Alternative pose comparisons for **SB-D10** (magenta) and **SB-D04** (orange) in the gp41 pocket (gray surface).

Another compound, **SB-C01**, contains an indole group which is positioned midway between Trp120 and Ile124 of the reference molecule (Fig. 4). Indoles form the basis of series of gp41 inhibitors recently reported by Zhou et al,[11] although in a different arrangement than that reported here. Of particular interest for **SB-C01** is the striking overlap of the carboxylic acid with that of the reference. Preliminary SAR studies were pursued by creating virtual analogues of **SB-C01** (Table 2, **M1**–**M8**) and energy-minimizing them in the gp41 site using a harmonic restraint tethered to the predicted binding pose (Fig. 4). Although the FPS_{ES} overlap for **SB-C01** with the reference was already high (0.99), a comparison of the VDW footprints (0.90) suggested interactions with residues Leu54c, Leu57c and Trp60c which lie along the edge of the gp41 pocket could be improved. Based on visual inspection of the predicted **SB-C01** pose, positions R1 and R2 (see Table 2) are natural points for SAR exploration.

Simple alkylations at R1 (**M1** and **M2**) were moderately successful in increasing the VDW footprint correlation and generating a more favorable DCE_{VDW+ES} score relative to the parent **SB-C01**. FPS_{VDW} scores increased from 0.90 to 0.92 while DCE_{VDW+ES} scores favorably increased from −1 to −2.5 kcal/mol. Importantly, the FPS_{ES} scores remained high and the low rmsds obtained after minimization indicates the **M1** and **M2** virtual analogs are as well-accommodated in the pocket as the parent **SB-C01**. In contrast, the same modifications at R2 (**M3**, **M4**) did not lead to noticeable improvement. Methylation (**M3**) had no effect while ethylation (**M4**) significantly reduced the FPS_{VDW} (0.90→0.66) and DCE_{VDW+ES} (−41.86→−32.98 kcal/mol) values compared to **SB-C01**. Further, the larger movement for **M4** (1.03 Å rmsd) upon minimization, compared to the other analogs tested suggests ethylation at R2 may have introduced an unfavorable interaction. In general, the analogs with the smallest rmsd movement yielded more favorable DCE_{VDW+ES} scores (Table 2). Initial attempts to increase favorable electrostatic interactions with Arg68c at the end of the gp41 pocket were also not fruitful. R3 modifications incorporating hydroxyl (**M5**, **M7**) or carboxylate (**M7**, **M8**) functionalities led to less favorable interactions with the exception of **M7** (R3 = CH_2OH), although the difference was negligible. Further studies will be needed with an expanded palate of functional groups. More extensive SAR based on all 7 actives shown in Figure 4 are in progress.

Finally, to further probe the stability of the predicted pose of **SB-C01**, molecular dynamics (MD) simulations were performed of the gp41-ligand complex using the program AMBER[23] with FF94SB[24] (protein), GAFF[25] (ligand), and TIP3P[26] (solvent) force fields. Sixteen 2-ns production simulations, using different random seeds, were performed with weak restraints on the protein backbone after an initial energy minimization and equilibration protocol with decreasing restraints. The simulations yielded a

Table 2
SB-C01 analogues, corresponding DCE scores, FPS scores, and movement (rmsd) after energy minimization

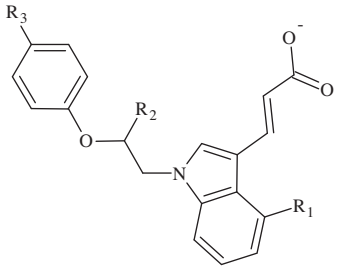

ID	R1	R2	R3	DCE_{VDW+ES}[a]	FPS_{VDW+ES}	FPS_{VDW}	FPS_{ES}	Rmsd
SB-C01	H	H	CH_3	−41.86	1.89	0.90	0.99	0.05
M1	CH_3	H	CH_3	−42.90	1.91	0.92	0.99	0.05
M2	CH_2CH_3	H	CH_3	−43.49	1.91	0.92	0.99	0.19
M3	H	CH_3	CH_3	−41.68	1.90	0.91	0.99	0.27
M4	H	CH_2CH_3	CH_3	−32.98	1.66	0.66	0.99	1.03
M5	H	H	OH	−41.79	1.89	0.90	0.99	0.06
M6	H	H	COO^-	−39.18	1.83	0.84	0.99	0.36
M7	H	H	CH_2OH	−42.02	1.88	0.89	0.99	0.16
M8	H	H	CH_2COO^-	−39.02	1.85	0.86	0.99	0.51

[a] DCE scores in kcal/mol, FPS scores are unitless, rmsd in Å.

low 2.3 Å average rmsd for the ligand providing further evidence the predicted **SB-C01** pose is compatible with the gp41 pocket. From another point of view, the MD-averaged FPS_{VDW} and FPS_{ES} similarity scores (using the original docked pose as reference) remain high (FPS >0.96) indicating the primary energetic signature also remains stable even when subjected to thermal fluctuations.

Figure 6 shows a binding site closeup from a representative MD simulation of the **SB-C01**/gp41 complex. Here, overlaid snapshots ($N = 10$) reveal a coordinated movement of the carboxylic acid and indole functionalities on **SB-C01** with Lys63a and Leu57c, respectively in the gp41 pocket. Relative to the original pose, the carboxylic acid alternates between a salt-bridge with Lys63a and an H-bond with Gln66a. Using a salt-bridge definition of $\leqslant$4.0 Å (carboxylic O···lysine N) the interaction was present 50.48% of the time. Interestingly, 9.42% of the time there is both a salt-bridge with Lys63a and an H-bond with Gln66a (2.5 Å definition).

In general, out of sixteen simulations, the most favorable FPS_{ES} scores were from runs in which the salt-bridge was formed more frequently. This is to be expected given that the Gln66a H-bond is not observed in the original **SB-C01** docked pose. For comparison, a 9-ns fully-solvated MD simulation (following protocols outlined in McGillick et al.[6]), of the C-helix peptide inhibitor C34 used here to create the reference, yielded the analogous salt-bridge with Lys63a 66.76% of the time. Interestingly, the C34 peptide simulation did not yield H-bonds with Gln66a. Thus, a possible strategy for inhibitor development would be to prevent or reduce the apparent slippage of **SB-C01** towards Gln66a observed in Figure 6 which could further increase similarity to reference. Studies to test this hypothesis are underway through the addition of functionality designed to promote VDW contact with Leu54c, Leu57c, Trp60c, and Gln66a.

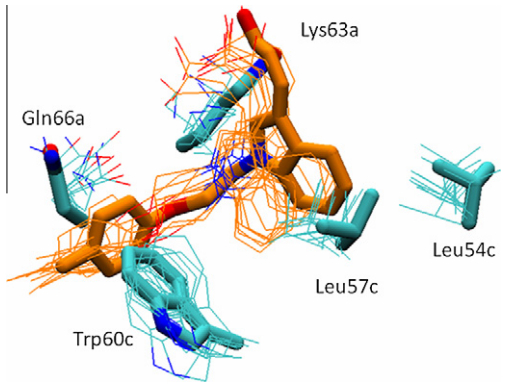

Figure 6. Starting position (stick) and location every 200 ps thereafter of **SB-C01** (orange) and key residues (cyan) from one 2 ns MD simulation.

In summary, in this report we performed a virtual screen of ca. 500,000 molecules against the hydrophobic pocket of HIVgp41. Using a new molecular footprinting method in conjunction with the standard DOCK energy score we selected 115 molecules for experimental testing. Seven inhibitors were identified with μM activity (K_i, IC_{50}) and reasonable cytotoxicity (CC_{50}) characteristics. Three of the seven inhibitors would not have been discovered without the use of footprints suggesting that the methodology may have utility for structure-based design. The fact that footprint-based screening leads to actives, in some cases, which share structurally related features to known gp41 inhibitors discovered via different methods[11,22] is particularly encouraging. Additional SAR studies are underway and extension of the method to incorporate reference-based footprints into lead refinement and de novo design protocols are planned.

Acknowledgments

Gratitude is expressed to Trent E. Balius, Sudipto Mukherjee, and William J. Allen for computational assistance and/or helpful discussions. This work was funded in part by the Stony Brook University Office of the Vice President for Research and the School of Medicine, and NIH grants R01GM083669 (R.C. R.) and R01GM087998 (M. G.). This research utilized resources at the New York Center for Computational Sciences at Stony Brook University/Brookhaven National Laboratory which is supported by the U.S. Department of Energy under Contract No. DE-AC02-98CH10886 and by the State of New York.

References and notes

1. Drugs@FDA website. http://www.accessdata.fda.gov/scripts/cder/drugsatfda/index.cfm (accessed Nov 3, 2011).
2. Davison, D. K.; Medinas, R. J.; Mosier, S. M.; Bowling, T. S.; Delmedico, M. K.; Dwyer, J. J.; Cammack, N.; Greenberg, M. L. AIDS 2006 - XVI International AIDS Conference. Abstract no. THPE0021.
3. Greenberg, M. L.; Cammack, N. J. *Antimicrob. Chemother.* **2004**, *54*, 333.
4. Melby, T.; Sista, P.; DeMasi, R.; Kirkland, T.; Roberts, N.; Salgo, M.; Heilek-Snyder, G.; Cammack, N.; Matthews, T. J.; Greenberg, M. L. *AIDS Res. Hum. Retrovir.* **2006**, *22*, 375.
5. Mink, M.; Mosier, S. M.; Janumpalli, S.; Davison, D.; Jin, L.; Melby, T.; Sista, P.; Erickson, J.; Lambert, D.; Stanfield-Oakley, S. A.; Salgo, M.; Cammack, N.; Matthews, T.; Greenberg, M. L. *J. Virol.* **2005**, *79*, 12447.
6. McGillick, B. E.; Balius, T. E.; Mukherjee, S.; Rizzo, R. C. *Biochemistry* **2010**, *49*, 3575.
7. Chan, D. C.; Chutkowski, C. T.; Kim, P. S. *Proc. Natl. Acad. Sci. U.S.A.* **1998**, *95*, 15613.
8. Cai, L.; Jiang, S. *ChemMedChem* **1813**, *2010*, 5.
9. Stewart, K. D.; Huth, J. R.; Ng, T. I.; McDaniel, K.; Hutchinson, R. N.; Stoll, V. S.; Mendoza, R. R.; Matayoshi, E. D.; Carrick, R.; Mo, H.; Severin, J.; Walter, K.; Richardson, P. L.; Barrett, L. W.; Meadows, R.; Anderson, S.; Kohlbrenner, W.; Maring, C.; Kempf, D. J.; Molla, A.; Olejniczak, E. T. *Bioorg. Med. Chem. Lett.* **2009**, *20*, 612.
10. Katritzky, A. R.; Tala, S. R.; Lu, H.; Vakulenko, A. V.; Chen, Q. Y.; Sivapackiam, J.; Pandya, K.; Jiang, S.; Debnath, A. K. *J. Med. Chem.* **2009**, *52*, 7631.

11. Zhou, G.; Wu, D.; Snyder, B.; Ptak, R. G.; Kaur, H.; Gochin, M. *J. Med. Chem.* **2011**, *54*, 7220.
12. Balius, T. E.; Mukherjee, S.; Rizzo, R. C. *J. Comput. Chem.* **2011**, *32*, 2273.
13. DOCK6.5, University of California at San Francisco, San Francisco, CA, 2011.
14. Chan, D. C.; Fass, D.; Berger, J. M.; Kim, P. S. *Cell* **1997**, *89*, 263.
15. Jiang, S.; Debnath, A. K. *Biochem. Biophys. Res. Commun.* **2000**, *270*, 153.
16. Irwin, J. J.; Shoichet, B. K. J. *Chem. Inf. Model* **2005**, *45*, 177.
17. Mukherjee, S.; Balius, T. E.; Rizzo, R. C. J. *Chem. Inf. Model* **1986**, *2010*, 50.
18. Brown, R. D.; Martin, Y. C. J. *Chem. Inf. Comput. Sci.* **1996**, *36*, 572.
19. MOE 2008.10, Chemical Computing Group Inc.
20. Cai, L.; Gochin, M. *Antimicrob. Agents Chemother.* **2007**, *51*, 2388.
21. Strockbine, B.; Rizzo, R. C. *Proteins: Struct. Funct. Bioinf.* **2007**, *67*, 630.
22. Jiang, S. B.; Lu, H.; Liu, S. W.; Zhao, Q.; He, Y. X.; Debnath, A. K. *Antimicrob. Agents Chemother.* **2004**, *48*, 4349.
23. Case, D. A.; Cheatham, T. E.; Darden, T.; Gohlke, H.; Luo, R., Jr; Onufriev, A.; Simmerling, C.; Wang, B.; Woods, R. J. *J. Comput. Chem.* **2005**, *26*, 1668.
24. Hornak, V.; Abel, R.; Okur, A.; Strockbine, B.; Roitberg, A.; Simmerling, C. *Proteins: Struct. Funct. Bioinf.* **2006**, *65*, 712.
25. Wang, J. M.; Wolf, R. M.; Caldwell, J. W.; Kollman, P. A.; Case, D. A. *J. Comput. Chem.* **2005**, *26*, 114.
26. Jorgensen, W. L.; Chandrasekhar, J.; Madura, J. D.; Impey, R. W.; Klein, M. L. *J. Chem. Phys.* **1983**, *79*, 926.